Nanoscale

ROYAL SOCIETY OF CHEMISTRY

PAPER

View Article Online
View Journal | View Issue

Check for updates

Cite this: *Nanoscale*, 2020, **12**, 12038

Wrinkle-induced highly conductive channels in graphene on SiO_2/Si substrates†

Rui-Song Ma, ‡[a,b] Jiajun Ma,‡[a,b] Jiahao Yan,[a,b] Liangmei Wu,[a,b] Wei Guo,[c] Shuai Wang,[c] Qing Huan,[a,b] Lihong Bao, *[a,b,d] Sokrates T. Pantelides[b,e] and Hong-Jun Gao [a,b,d]

Received 19th February 2020,
Accepted 6th May 2020

DOI: 10.1039/d0nr01406k

rsc.li/nanoscale

A graphene wrinkle is a quasi-one-dimensional structure and can alter the intrinsic physical and chemical activity, modify the band structure and introduce transport anisotropy in graphene thin films. However, the quasi-one-dimensional electrical transport contribution of wrinkles to the whole graphene films compared to that of the two-dimensional flat graphene nearby has still been elusive. Here, we report measurements of relatively high conductivity in micrometer-wide graphene wrinkles on SiO_2/Si substrates using an ultrahigh vacuum (UHV) four-probe scanning tunneling microscope. Combining the experimental results with resistor network simulations, the wrinkle conductivity at the charge neutrality point shows a much higher conductivity up to ~33.6 times compared to that of the flat monolayer region. The high conductivity can be attributed not only to the wrinkled multilayer structure but also to the large strain gradients located mainly in the boundary area. This method can also be extended to evaluate the electrical-transport properties of wrinkled structures in other two-dimensional materials.

Introduction

Graphene, as the first discovered two-dimensional (2D) material with honeycomb structure, was mechanically exfoliated from bulk graphite using Scotch tape in 2004.[1,2] With excellent mechanical,[3] electrical,[4] and optical properties,[5] it shows prospects of promising applications in terms of field-effect transistors,[6] optoelectronic devices,[7] and flexible and transparent electrodes.[8] Other than mechanical exfoliation, methods for preparing large-area and high-quality graphene include chemical vapor deposition (CVD),[9] reduction of graphene oxide,[10] epitaxial growth on SiC[11] and single crystals of noble metals,[12–15] *etc*. Due to the thermodynamic requirement, strictly 2D graphene does not exist and therefore, pronounced out-of-plane deformations are present in the form of ripples even in suspended graphene with a height of up to 1 nm.[16] Wrinkled structures are formed on the substrate during the preparation and transfer process,[17] through which layer–layer interactions can lower the total energy of the system.[18] The most observed wrinkle structure is collapsed trilayer graphene, in which the folded region shows large curvature and apparent height.[19–22] The distribution of wrinkle width is wide, ranging from ~10 nm to several micrometres, while the length can be one order of magnitude larger.[23] Therefore, a wrinkle can be regarded as a quasi-one-dimensional structure within 2D graphene films.

For pristine monolayer graphene, the nearest two carbon atoms in the honeycomb lattice are bound together by the π bond and electrons can move freely in-plane. For multilayer graphene (bilayer, trilayer or more), the stacking order can be AB/ABC or turbostratic due to the van der Waals interactions and interlayer tunneling allowing carrier transport between layers.[17] As for the graphene wrinkle, it can be considered as multiple-stacked layers jointed by a folded region with a large curvature, by which the band structure is significantly tuned.[20,21,24,25] Previous scanning tunneling microscopy (STM) studies suggested that the local curvature of the wrinkle can break the six-fold symmetry of the graphene lattice and lead to the presence of midgap states in the neutrality point.[26,27] For a sub-5 nm graphene wrinkle on Ni (111), scanning tunneling spectroscopy (STS) results revealed

[a]*Institute of Physics, Chinese Academy of Sciences, PO Box 603, Beijing 100190, People's Republic of China. E-mail: lhbao@iphy.ac.cn*
[b]*University of Chinese Academy of Sciences & CAS Center for Excellence in Topological Quantum Computation, Chinese Academy of Sciences, PO Box 603, Beijing 100190, People's Republic of China*
[c]*Key Laboratory of Material Chemistry for Energy Conversion and Storage, Ministry of Education, School of Chemistry and Chemical Engineering, Huazhong University of Science and Technology, Wuhan, 430074, People's Republic of China*
[d]*Songshan Lake Materials Laboratory, Dongguan, Guangdong 523808, People's Republic of China*
[e]*Department of Physics and Astronomy and Department of Electrical Engineering and Computer Science, Vanderbilt University, Nashville, Tennessee 37235, USA*
† Electronic supplementary information (ESI) available. See DOI: 10.1039/d0nr01406k
‡ These authors contributed equally to this work.

bandgap opening and a one-dimensional van Hove singularity, showing the possibility of controlling the electronic band structure of graphene by engineering the geometric structure.[28] As for the nanoscale double-folded wrinkle in monolayer graphene on SiO_2/Si, pseudo Landau levels were observed in STS, which are caused by a gradient-strain-induced pseudomagnetic field of up to ∼42 T.[20] In both the systems above, dI/dV spectra recorded in the wrinkled region were pronouncedly higher than those in the pristine monolayer area.[20,28] In addition, DFT calculations showed that the charge density distributions of the enhanced up-dispersed and the down-dispersed states are mainly distributed within the wrinkled trilayer area.[20,21] Therefore, compared with their flat counterpart, the graphene wrinkles give rise to significant changes in the energy band structures and electrical properties, and show new application prospects in field effect transistors and flexible electronics.[23]

Previous studies on the electrical transport properties of graphene with wrinkled structures treated the wrinkle as a line-defect like a grain boundary, which degrades the conductivity and mobility of carriers traversing it.[29–33] The reduction in electrical figures of merit for the transverse transport through wrinkles is mainly attributed to carrier scattering by flexural phonons that stem from the corrugations.[34,35] Furthermore, formation of graphene wrinkles can lead to inhomogeneous charge distribution and local variation of surface potential, forming potential barriers for electrons.[32,36,37] A distinct anisotropy in conductivity of wrinkled graphene was observed and transport along the folded wrinkles showed much better electrical performance than that across the wrinkles.[34,37–40] Wu *et al.* found that there exists strong confinement in the graphene wrinkle and electronic waveguides are formed in the direction parallel to the fold axis.[41] All these results indicate that wrinkles are one dimensional (1D) highly conductive channels and can be useful for constructing electronic devices. However, previous investigations were mainly performed by conventional two- and four-terminal measurements, in which the microfabrication process inevitably introduces undesirable contamination, irreversibly causes damage, and changes the intrinsic electrical properties.[34,38–41] Furthermore, 1D electrical transport contribution to the whole graphene films compared to that of 2D flat graphene nearby has not been isolated yet.

In this work, we report wrinkle-induced highly conductive channels in millimeter-scale graphene, typically 1 mm in size, using a UHV four-probe STM system. By performing variable-spacing four-probe measurements away from and along the graphene wrinkles, it is found that the presence of wrinkles leads to breaking down of the 2D transport nature of pristine graphene. Collinear four-probe measurement with fixed spacing shows that the introduction of wrinkles results in a much higher conductivity compared to that of the monolayer regions on both sides. Using a resistor network simulation, the conductivity in the wrinkled area is extracted, which can be up to ∼33.6 times higher than that in the flat monolayer region. Both the multilayer structure and large strain presented in the wrinkled area can be the cause for the high conductivity within the quasi 1D channels.

Experimental section

The millimeter-scale graphene samples were grown on Cu foil by the CVD method and then transferred onto a Si substrate with a 300 nm SiO_2 dielectric layer by the poly(methyl methacrylate)-assisted method.[9] Atomic-force-microscopy (AFM) characterization was performed under ambient conditions using a Nanoscope IIIa SPM (Digital Instruments) and all data were collected in tapping mode. Raman mapping was obtained using a Horiba HR Evolution Raman microscope system under ambient conditions. The setup parameters are a 532 nm laser wavelength, a 0.90/100× objective and a 1 μm beam spot size. The STM/STS experiments and electrical transport measurements were performed using a home-designed UHV 4P-STM system running at a base pressure of about 5.0×10^{-10} mbar.[42] The STS results were obtained using a lock-in amplifier with a typical sinusoidal modulation of 5.9 meV (rms) at 973 Hz. The dI/dV spectra were recorded from an average of 100 individual curves obtained continuously at the corresponding positions. In the load-lock chamber, the graphene@SiO_2/Si samples were annealed at 200 °C for 24 hours at a pressure of $\sim 1 \times 10^{-8}$ mbar. During the STM experiments, a chemically etched W tip operated in constant-current mode, while a chemically etched gold tip contacts the sample as the bias electrode. All four-probe electrical transport characterization studies were performed at room temperature using chemically etched gold tips and a Keithley 4200-SCS system. The real-time capacitance signals between the probes and the gate were monitored as feedback during the probe approaching process for the conductive sample on dielectric substrate, such as graphene@SiO_2/Si in this paper. In order to reduce the interference coming from graphene edges and wrinkles, the probe distances from the wrinkles and the edges were set as at least ∼1.6 times larger than the probe distances with a measuring error under ±5%.[43] Since the wrinkles can also interfere with each other, we performed four-probe measurements on isolated wrinkles which are at least ∼100 μm away from others. The carrier densities of graphene on the SiO_2/Si substrate can be tuned by applying voltage to the heavily doped Si (P++ Si) layer.

Results and discussion

The extended graphene wrinkles were formed during the transfer process and their width and length are micron-scale and millimeter-scale, respectively. A typical graphene wrinkle (labeled as wrinkle-1) of ∼3 μm wide is shown in Fig. 1(a) and the corresponding large-area AFM images are shown in Fig. 1(b). The wrinkle is embedded in monolayer graphene regions with a thickness of ∼1.0 nm as confirmed by AFM,[44] as shown in Fig. S1(a) in the ESI.† The monolayer nature is also confirmed by Raman characterization (Fig. S1(b) in the

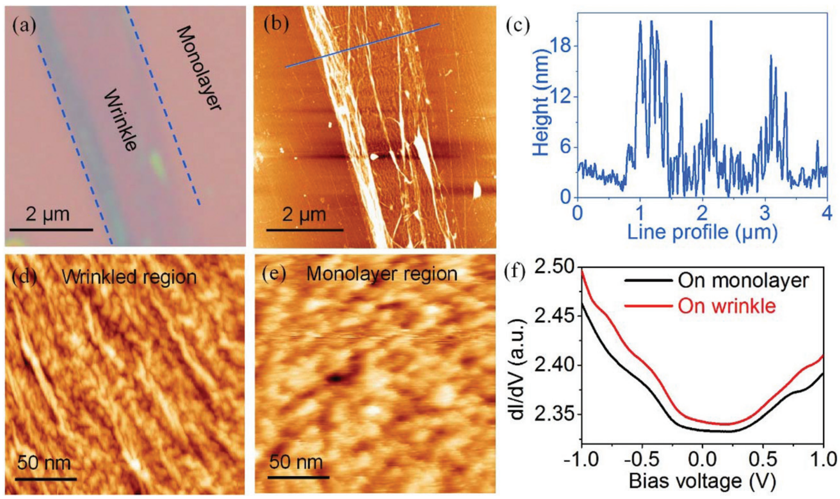

Fig. 1 Optical, AFM and STM characterization of the graphene wrinkle. (a) Optical micrograph of one typical graphene wrinkle on the SiO_2 substrate. (b) AFM image of the graphene wrinkle in (a). (c) The line profile along the blue line in (b). (d) STM image of the graphene wrinkle on the Si/SiO_2 substrate. The main direction of the small wrinkles is in parallel with the large wrinkle. (e) The STM image of the monolayer graphene area on the Si/SiO_2 substrate. No orientation preference is observed in the unwrinkled region. (f) STS results on the wrinkle (in red) and the monolayer graphene (in black), in which the former is distinctly higher than the latter. Each spectrum is an average of 100 neighboring spectra. STM imaging parameters: I_t = 3 nA and V_{sample} = −300 mV.

ESI†). According to the line profile shown in Fig. 1(c), the wrinkled area shows a much higher thickness compared to flat monolayers and an averaged wrinkle thickness is ~7.5 nm. As previously reported, in the folding structure, the wrinkle can be composed of three, five, or more layers, where the folding regions show a much larger curvature like carbon nanotubes.[20,21,39] In addition, the layers were not closely stacked due to the curved structures.[28] As can be seen in Fig. 1(c), the boundary sites are much higher than the middle area inside the wrinkle, which possesses larger curvature and has been also observed in sub-micro-scale wrinkles.[39] The micron-scale wrinkle is composed of many nm-scale wrinkles, the main directions of which are in parallel with the larger one, as shown in the STM image (Fig. 1(d)). In addition, we also performed STM characterization on the monolayer area in which no specific orientation is present (Fig. 1(e)). As shown in Fig. 1(f), our STS results also reveal that the local density of states at the wrinkled area is distinctly higher than that in the flat monolayer region, which is in accordance with previous studies.[20,28]

In the four-probe collinear measurement, the probes are arranged along a line, in which probes 1 & 4 are used to inject current (I1 and G4) to the sample, while probes 2 & 3 (V2 and V3) are used to measure the potential difference on the sample surface.[43] The measured resistances of the sample with homogeneous conductivity σ are defined by the potential difference (V23 = V2 − V3) over the injected current (V23/I1), which are sensitive to the sample dimensionality and the distance between the probes. The probes are usually equally spaced with the current probes at the outside.[43] In a specific case, the distance between probes 1 and 4 is fixed to 3 (a.u.), while V2 is positioned between them at a distance of 1 (a.u.) from probe 4 (Fig. 2(a and b)). Probe 3 is movable and the distance between G4 and V3 is x (a.u.). For materials with different dimensionalities, the measured resistance will follow a specific relationship as a function of x, as shown in Fig. S2 in the ESI.† In particular, when x is 3 for the 2D case, the measured resistance is equal to zero since V2 and V3 are the same.

Using this measurement configuration, the dimensionality of transport behavior has been probed on thin Al foil and the bulk bismuth sample.[45] In our case, the unit of the probe distance is set as 30 μm and variable-spacing four-probe measurements were performed both away from and along graphene wrinkles, as illustrated in Fig. 2(a) and (b), respectively. In the former configuration, the measured resistances as a function of x follow the 2D behavior quite well (red curve), as shown in Fig. 2(c). As for the latter configuration, the measured resistances deviate from the 2D scaling regime and no negative values are presented (Fig. 2(d)). Therefore, the presence of a wrinkle breaks the original 2D transport properties in graphene and introduces additional one-dimensional contribution to the electrical transport.[46]

Previous studies treated a wrinkle as a kind of defect like a graphene grain boundary, which can build a transport barrier, thus degrading the transport properties in terms of conductivity and carrier mobility when the electrons pass through it, as shown in Figs. S4(a) and (c) in the ESI.†[30–33,47] In order to study the electrical transport properties along the quasi-one-dimensional channel, collinear four-probe measurements with equal spacing (~60 μm) are performed both away from and along wrinkle-1, as schematically shown in Fig. 3(a) and (b), respectively. The gate-tunable conductivities and conductivity ratios of the two setups are shown in Fig. 3(c) and (d), respectively. It shows that the conductivities along the wrinkle (represented by $\sigma_{\square\text{along-w}}$) are several times higher than those in the pristine monolayer region ($\sigma_{\square\text{m}}$), especially at a high gate

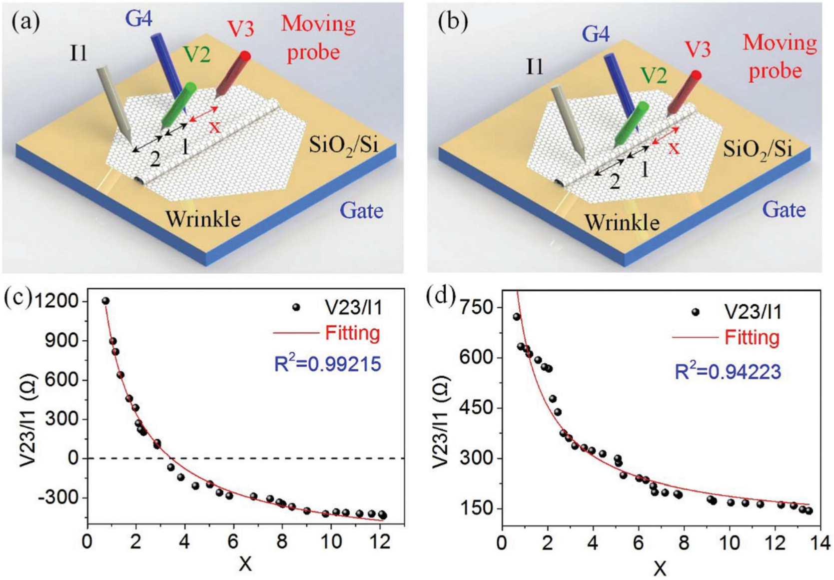

Fig. 2 Variable-spacing four-probe measurements away from and along a graphene wrinkle. (a and b) Schematic illustration (not to scale) of four-probe collinear measurements away from and along a graphene wrinkle, respectively. Probes 1, 2 and 4 are fixed, while probe 3 is movable. The distance between probes 3 and 4 is set as *x*. (c and d) The measured resistance (V23/I1) as a function of *x* at zero gate bias for the cases shown in (a) and (b), respectively. The black dash line in (c) shows the zero position of the measured resistance. The red solid lines show the fitting curves based on the 2D case.

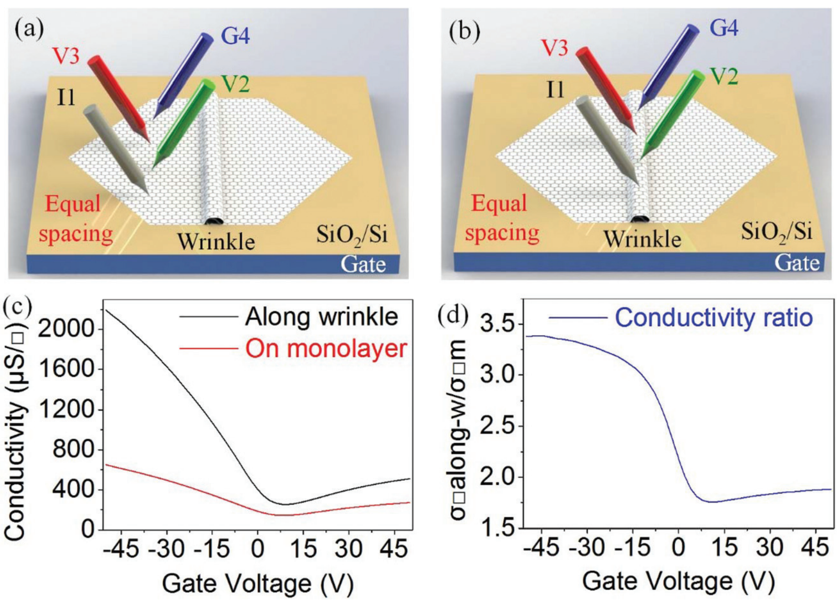

Fig. 3 Collinear four-probe measurement away from and along the graphene wrinkle with equal spacing. (a and b) Schematic illustration (not to scale) of four-probe collinear measurements away from and along a graphene wrinkle, respectively. The four probes are arranged along a line with equal spacing (60 μm). (c) Gate-tunable conductivity for the cases away from and along the graphene wrinkle-1 as shown in (a) and (b). The curves are averaged by eight measurements at different positions in each case. (d) Conductivity ratio of four-probe measurements along the graphene wrinkle ($\sigma_{\square\text{along-w}}$) and on the monolayer area ($\sigma_{\square\text{m}}$).

voltage range. Therefore, the presence of a quasi-one-dimensional wrinkle leads to a higher conductivity in two-dimensional graphene film. In addition, the charge neutral points for both cases are located at the same position, indicating that no observable doping effect is introduced by the wrinkle. The same four-probe electrical measurements on other wrinkles (labeled as wrinkles 2–5) show similar results, as shown in Fig. S4 and S5 (see the ESI†).

Since the wrinkles are embedded within the monolayer graphene, the conductivity along the wrinkle in the four-probe

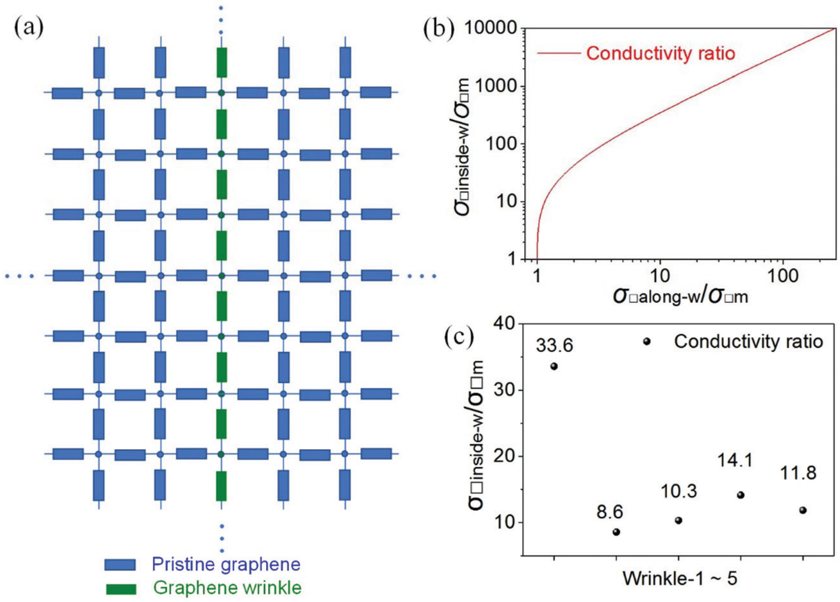

Fig. 4 Resistor network simulation. (a) Schematic illustration of resistor network simulation for four-probe collinear measurements along a graphene wrinkle. The blue and green resistors represent the pristine graphene and graphene wrinkle, respectively. (b) Simulated conductivity ratio of four-probe measurements along the wrinkle and on the monolayer region *vs.* conductivity ratio of the wrinkled area and the monolayer region. (c) Conductivity ratios of five graphene wrinkles labeled 1–5 at the charge neutral point in this paper.

measurements is determined by both the conductivity inside the wrinkle ($\sigma_{\square\text{inside-w}}$) and that of flat monolayer graphene. In order to estimate the contribution solely from the wrinkle, resistor network simulation is employed to simulate the four-probe collinear measurements, as shown in Fig. 4(a). Therein, green and light blue resistors represent the graphene wrinkle and pristine graphene, respectively. In a resistor network with a constant current source, the potential distribution is merely determined by the relative conductivity.[33] That is to say, the ratio of $\sigma_{\square\text{inside-w}}$ to $\sigma_{\square\text{m}}$ results in the potential profile in the four-probe case if the injected current is constant. For the experimental results, $\sigma_{\square\text{along-w}}$ and $\sigma_{\square\text{m}}$ can be directly obtained from the four-probe measurements. Based on the resistor network simulation (see details in the ESI†), $\sigma_{\square\text{inside-w}}/\sigma_{\square\text{m}}$ can be extracted from $\sigma_{\square\text{along-w}}/\sigma_{\square\text{m}}$, as shown in Fig. 4(b). Accordingly, for the case in Fig. 3, the presence of wrinkle-1 can lead to an increased conductivity by up to ~1.76 times at the charge neutral point, which means the conductivity solely in the wrinkled region is ~33.6 times higher than that in pristine graphene (Fig. 4(c)). The conductivity ratios of wrinkles 2–5 at the charge neutral point are also shown in Fig. 4(c), wherein all of them show about one order higher conductivity. Based on these ratios, the conductivity solely in the wrinkled region can be extracted which is on the order of several mS $\square^{-1}$, as shown in Fig. S6.†

As revealed in the AFM and STM images shown in Fig. 1(b–d), the height and thus structures in wrinkle-1 vary from place to place, while the averaged wrinkle thickness is about 7.5 nm. Previous studies showed that the wrinkles are composed of multi-folded graphene layers, in which an averaged layer thickness is about 0.5 nm in trilayer or five-layer wrinkle structures.[21] As for wrinkle-1 with inhomogeneous structures, it is approximately composed of 15 layers on average. As a consequence, for carrier transport along the wrinkled graphene area, the multilayer graphene structure can provide additional transport channels, thus leading to a much lower resistance than that in the flat monolayer region.[39] The different conductivity of the five wrinkles can be mainly attributed to the variations of the width and height in the wrinkled area.[39] The wider and higher the wrinkle, the more the likely presence of transport channels, which can promote electron transport and increase electrical conductivity. Among the five wrinkles, the averaged lateral size of wrinkle-1 is the largest (~3 μm × ~7.5 nm), and it shows the highest conductivity. Since the width and height of graphene wrinkles span a wide range, the statistical spread of the conductivity is large.

As is known, both strain and doping can modify the band structure and influence the electrical transport properties of graphene.[48] It was reported that for a narrow graphene wrinkle on the SiO_2/Si substrate, pronounced and nearly equally separated pseudo Landau levels were observed in the dI/dV spectra, which are caused by a gradient-strain-induced pseudo magnetic field.[20] Lee *et al.* reported that mechanical strain and charge doping in graphene can be separated *via* mapping of Raman 2D and G modes.[49] Raman characterization studies of 2D and G peak positions are performed on wrinkle-1, as shown in Fig. 5(a–c). Previous studies showed that both hole and electron doping will lead to upshift of Raman G peaks.[50] However, only downshift is observed in our case. Furthermore, based on the gate-tunable conductivity measurements, no distinct shift in the charge neutral point or doping preference is shown, compared with the unwrinkled graphene area. Both

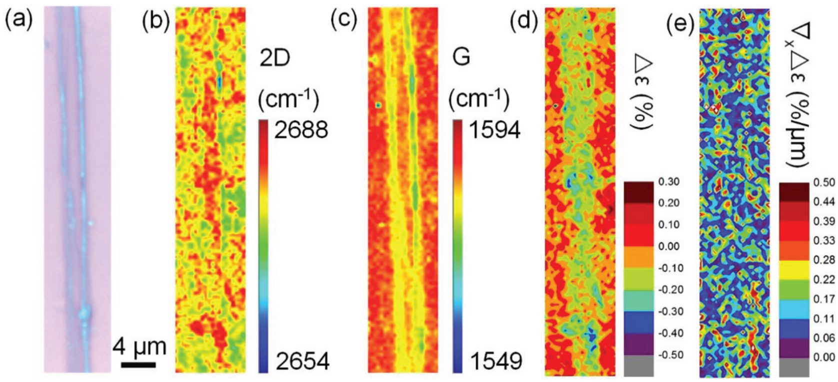

Fig. 5 Raman characterization of the graphene wrinkled area. (a) Optical micrograph of the characterized graphene wrinkle-1. (b and c) Raman maps of the 2D and G peak positions of the graphene wrinkle shown in (a). (d) Contour map for graphene strain extracted from the mapping results shown in (b) and (c). The wrinkled areas show a compressive strain of up to 0.4%, while the monolayer regions near the wrinkle present a tensile strain of up to 0.3%. (e) Distribution of the strain gradient along the direction perpendicular to the wrinkle. The large strain gradients are mainly located at the wrinkle boundary.

results exclude the possibility of doping in causing the increased conductivity.

Based on the vector deposition method proposed by Lee *et al.* (see details in the ESI†), strain variations are estimated as shown in Fig. 5(d).[49] The wrinkled regions show a compressive strain of up to 0.4%, while the monolayer regions near wrinkle-1 present a tensile strain of up to 0.3%, in agreement with the sub-micron-scale wrinkles.[37] Accordingly, the strain polarity is reversed in the wrinkle boundary position, and therefore large strain gradients are mainly distributed in the boundary area with larger curvatures, as confirmed in Fig. 5(e). In addition, Raman characterization studies of wrinkle-2 reveal a similar polarity of strain distributions, as shown in Fig. S8 in the ESI.† The strain variations of the five wrinkles are significant, in which the highest compressive strain inside the wrinkle can be up to ~0.5% and the highest tensile strain near the wrinkle can reach ~0.3%, as summarized in Fig. S9 in the ESI.† Such strong variations in strain distributions (Fig. 5 and Fig. S8, S9 in the ESI†) result from the difference in inhomogeneous morphologies and local curved structures between regions both inside and near the wrinkle, which is confirmed by the AFM and STM images shown in Fig. 1(b–d). Previous theoretical studies revealed that local strain can effectively engineer the electronic structure of graphene by considering nearest-neighbor hopping amplitude changes and be used to generate 1D channels, surface states, and confinement.[25] Furthermore, the calculations showed that the charge density distributions of the enhanced up-dispersed and the down-dispersed states are mainly distributed within the wrinkle with larger curvature.[20,21] Therefore, besides the wrinkle dimension, strain gradients should also be an important factor for the enhanced conductivity of wrinkles. Since the conductivity is positively correlated with strain, local variations of levels of strain in the wrinkled region can be a minor cause for the different conductivity of the five wrinkles. To pick out wrinkles with possibly higher conductivity, levels of strain distributions should be characterized individually.

In general, due to the multilayer channels and strain-enhanced electronic states, the pseudo-one-dimensional wrinkles provide highly conductive channels in two-dimensional graphene films and can be used for electronic applications, such as interconnecting channels in chips. Additionally, it has already been addressed that periodically 1D wrinkles can be fabricated by transferring graphene onto substrates with organized microstructure or pre-stretched polymer substrates, which is important for manufacturing high-speed and flexible electronic devices.[17,51] Beyond graphene, wrinkles can also be used to control the band structure of other two-dimensional materials, such as MoS_2,[52] and therefore our four-probe method can be extended to characterize wrinkle-induced electrical transport properties in these systems.

In conclusion, we demonstrate direct probing of conductivity enhancement in quasi-1D wrinkles within millimeter-sized graphene on SiO_2 substrates using a UHV four-probe STM system. The micro-scale graphene wrinkles are composed of many nano-scale wrinkles, the main orientations of which are nearly in parallel. According to the variable-spacing four-probe measurements away from and along the graphene wrinkles, it is revealed that the introduction of wrinkles strongly disturbs the 2D transport behavior of pristine graphene. Collinear four-probe measurements show that the conductivities along the wrinkles are distinctly higher than those along the flat monolayer area. Based on the resistor network simulation, the conductivity inside the wrinkled region can be 33.6 times higher than that in the non-wrinkled region, which can be attributed to the multilayer configuration and large strain gradients shown in the wrinkled area. Our results help to pave the way toward practical applications with wrinkled graphene as electrodes in electrical devices and can be used to probe the corrugation-induced effects in other 2D materials.

Conflicts of interest

There are no conflicts of interest to declare.

Acknowledgements

This work was supported by grants from the National Key Research & Development Projects of China (No. 2016YFA0202300 and 2018FYA0305800), the National Natural Science Foundation of China (No. 61674170 and 61888802), the K. C. Wong Education Foundation, the Strategic Priority Research Program of Chinese Academy of Sciences (No. XDB30000000 and XDB28000000), and the Youth Innovation Promotion Association of CAS (20150005). Work at Vanderbilt (S.T.P.) was supported by the McMinn Endowment.

References

1 K. S. Novoselov, A. K. Geim, S. V. Morozov, D. Jiang, Y. Zhang, S. V. Dubonos, I. V. Grigorieva and A. A. Firsov, *Science*, 2004, **306**, 666–669.
2 A. K. Geim and K. S. Novoselov, *Nat. Mater.*, 2007, **6**, 183–191.
3 C. Lee, X. D. Wei, J. W. Kysar and J. Hone, *Science*, 2008, **321**, 385–388.
4 S. V. Morozov, K. S. Novoselov, M. I. Katsnelson, F. Schedin, D. C. Elias, J. A. Jaszczak and A. K. Geim, *Phys. Rev. Lett.*, 2008, **100**, 016602.
5 L. A. Falkovsky, *J. Phys.: Conf. Ser.*, 2008, **129**, 012004.
6 F. Schwierz, *Nat. Nanotechnol.*, 2010, **5**, 487–496.
7 F. Bonaccorso, Z. Sun, T. Hasan and A. C. Ferrari, *Nat. Photonics*, 2010, **4**, 611–622.
8 S. Bae, H. Kim, Y. Lee, X. F. Xu, J.-S. Park, Y. Zheng, J. Balakrishnan, T. Lei, H. R. Kim, Y. I. Song, Y.-J. Kim, K. S. Kim, B. Özyilmaz, J.-H. Ahn, B. H. Hong and S. Iijima, *Nat. Nanotechnol.*, 2010, **5**, 574–578.
9 W. Guo, F. Jing, J. Xiao, C. Zhou, Y. Lin and S. Wang, *Adv. Mater.*, 2016, **28**, 3152–3158.
10 S. Pei and H.-M. Cheng, *Carbon*, 2012, **50**, 3210–3228.
11 C. Berger, Z. Song, X. Li, X. Wu, N. Brown, C. Naud, D. Mayou, T. Li, J. Hass, A. N. Marchenkov, E. H. Conrad, P. N. First and W. A. de Heer, *Science*, 2006, **312**, 1191.
12 Y. Pan, H. Zhang, D. Shi, J. Sun, S. Du, F. Liu and H.-J. Gao, *Adv. Mater.*, 2009, **21**, 2777–2780.
13 Y. Pan, D.-X. Shi and H.-J. Gao, *Chin. Phys.*, 2007, **16**, 3151–3153.
14 J. Mao, L. Huang, Y. Pan, M. Gao, J. He, H. Zhou, H. Guo, Y. Tian, Q. Zou, L. Zhang, H. Zhang, Y. Wang, S. Du, X. Zhou, A. H. Castro Neto and H.-J. Gao, *Appl. Phys. Lett.*, 2012, **100**, 093101.
15 G. Li, H. Zhou, L. Pan, Y. Zhang, L. Huang, W. Xu, S. Du, M. Ouyang, A. C. Ferrari and H.-J. Gao, *J. Am. Chem. Soc.*, 2015, **137**, 7099–7103.
16 J. C. Meyer, A. K. Geim, M. I. Katsnelson, K. S. Novoselov, T. J. Booth and S. Roth, *Nature*, 2007, **446**, 60.
17 W. Chen, X. Gui, L. Yang, H. Zhu and Z. Tang, *Nanoscale Horiz.*, 2019, **4**, 291–320.
18 L. X. Benedict, N. G. Chopra, M. L. Cohen, A. Zettl, S. G. Louie and V. H. Crespi, *Chem. Phys. Lett.*, 1998, **286**, 490–496.
19 F. Long, R. Yasaei, R. Sanoj, W. Yao, P. Kral, A. Salehi-Khojin and R. Shahbazian-Yassar, *ACS Appl. Mater. Interfaces*, 2016, **8**, 18360–18366.
20 C. Ma, X. Sun, H. Du, J. Wang, M. Tian, A. Zhao, Y. Yamauchi and B. Wang, *Nano Lett.*, 2018, **18**, 6710–6718.
21 K. Kim, Z. Lee, B. D. Malone, K. T. Chan, B. Alemán, W. Regan, W. Gannett, M. F. Crommie, M. L. Cohen and A. Zettl, *Phys. Rev. B: Condens. Matter Mater. Phys.*, 2011, **83**, 245433.
22 S. U. Yu, B. Park, Y. Cho, S. Hyun, J. K. Kim and K. S. Kim, *ACS Nano*, 2014, **8**, 8662–8668.
23 S. Deng and V. Berry, *Mater. Today*, 2016, **19**, 197–212.
24 I. F. Herbut, V. Juričić and O. Vafek, *Phys. Rev. Lett.*, 2008, **100**, 046403.
25 V. M. Pereira and A. H. Castro Neto, *Phys. Rev. Lett.*, 2009, **103**, 046801.
26 Y. F. Zhang, T. Gao, Y. B. Gao, S. B. Xie, Q. Q. Ji, K. Yan, H. L. Peng and Z. F. Liu, *ACS Nano*, 2011, **5**, 4014–4022.
27 K. Xu, P. Cao and J. R. Heath, *Nano Lett.*, 2009, **9**, 4446–4451.
28 H. Lim, J. Jung, R. S. Ruoff and Y. Kim, *Nat. Commun.*, 2015, **6**, 8601.
29 K. L. Grosse, V. E. Dorgan, D. Estrada, J. D. Wood, I. Vlassiouk, G. Eres, J. W. Lyding, W. P. King and E. Pop, *Appl. Phys. Lett.*, 2014, **105**, 143109.
30 P. Willke, M. A. Schneider and M. Wenderoth, *Ann. Phys.*, 2017, **529**, 1700003.
31 P. Willke, C. Moehle, A. Sinterhauf, T. Kotzott, H. K. Yu, A. Wodtke and M. Wenderoth, *Carbon*, 2016, **102**, 470–476.
32 B. Vasic, A. Zurutuza and R. Gajic, *Carbon*, 2016, **102**, 304–310.
33 K. W. Clark, X. G. Zhang, I. V. Vlassiouk, G. He, R. M. Feenstra and A.-P. Li, *ACS Nano*, 2013, **7**, 7956–7966.
34 G.-X. Ni, Y. Zheng, S. Bae, H. R. Kim, A. Pachoud, Y. S. Kim, C.-L. Tan, D. Im, J.-H. Ahn, B. H. Hong and B. Özyilmaz, *ACS Nano*, 2012, **6**, 1158–1164.
35 P. Xu, M. Neek-Amal, S. D. Barber, J. K. Schoelz, M. L. Ackerman, P. M. Thibado, A. Sadeghi and F. M. Peeters, *Nat. Commun.*, 2014, **5**, 3720.
36 F. Guinea, M. I. Katsnelson and M. A. H. Vozmediano, *Phys. Rev. B: Condens. Matter Mater. Phys.*, 2008, **77**, 075422.
37 T. Hallam, A. Shakouri, E. Poliani, A. P. Rooney, I. Ivanov, A. Potie, H. K. Taylor, M. Bonn, D. Turchinovich, S. J. Haigh, J. Maultzsch and G. S. Duesberg, *Nano Lett.*, 2015, **15**, 857–863.
38 D. Zhang, Z. Jin, J. Shi, P. Ma, S. Peng, X. Liu and T. Ye, *Small*, 2014, **10**, 1761–1764.
39 W. J. Zhu, T. Low, V. Perebeinos, A. A. Bol, Y. Zhu, H. G. Yan, J. Tersoff and P. Avouris, *Nano Lett.*, 2012, **12**, 3431–3436.
40 S. Deng, E. Gao, Y. Wang, S. Sen, S. T. Sreenivasan, S. Behura, P. Kral, Z. Xu and V. Berry, *ACS Nano*, 2016, **10**, 8403–8412.
41 Y. Wu, D. Zhai, C. Pan, B. Cheng, T. Taniguchi, K. Watanabe, N. Sandler and M. Bockrath, *Nano Lett.*, 2018, **18**, 64–69.

42 R. Ma, Q. Huan, L. Wu, J. Yan, Q. Zou, A. Wang, C. A. Bobisch, L. Bao and H.-J. Gao, *Rev. Sci. Instrum.*, 2017, **88**, 063704.
43 I. Miccoli, F. Edler, H. Pfnur and C. Tegenkamp, *J. Phys.: Condens. Matter*, 2015, **27**, 223201.
44 C. J. Shearer, A. D. Slattery, A. J. Stapleton, J. G. Shapter and C. T. Gibson, *Nanotechnology*, 2016, **27**, 125704.
45 S. B. Kjeldby, O. M. Evenstad, S. P. Cooil and J. W. Wells, *J. Phys.: Condens. Matter*, 2017, **29**, 394008.
46 M. R. Lotz, M. Boll, O. Hansen, D. Kjaer, P. Boggild and D. H. Petersen, *Appl. Phys. Lett.*, 2014, **105**, 053115.
47 R. Ma, Q. Huan, L. Wu, J. Yan, W. Guo, Y.-Y. Zhang, S. Wang, L. Bao, Y. Liu, S. Du, S. T. Pantelides and H.-J. Gao, *Nano Lett.*, 2017, **17**, 5291–5296.
48 A. H. Castro Neto, F. Guinea, N. M. R. Peres, K. S. Novoselov and A. K. Geim, *Rev. Mod. Phys.*, 2009, **81**, 109–162.
49 J. E. Lee, G. Ahn, J. Shim, Y. S. Lee and S. Ryu, *Nat. Commun.*, 2012, **3**, 1024.
50 A. Das, S. Pisana, B. Chakraborty, S. Piscanec, S. K. Saha, U. V. Waghmare, K. S. Novoselov, H. R. Krishnamurthy, A. K. Geim, A. C. Ferrari and A. K. Sood, *Nat. Nanotechnol.*, 2008, **3**, 210.
51 B. Pacakova, T. Verhagen, M. Bousa, U. Huebner, J. Vejpravova, M. Kalbac and O. Frank, *Sci. Rep.*, 2017, **7**, 10003.
52 A. Castellanos-Gomez, R. Roldán, E. Cappelluti, M. Buscema, F. Guinea, H. S. J. van der Zant and G. A. Steele, *Nano Lett.*, 2013, **13**, 5361–5366.